Research paper

Effect of high temperature and accelerated aging in high density micro-concrete

Thomas, C.*[a]; Tamayo, P.[a]; Setién, J.[a]; Ferreño, D.[a]; Polanco, J.A.[a]; Rico, J.[b]

[a] LADICIM (Laboratory of Materials Science and Engineering Division), University of Cantabria. E.T.S. de Ingenieros de Caminos, Canales y Puertos, Av./Los Castros 44, 39005 Santander, Spain.
[b] INGECID S.L. (Ingeniería de la Construcción, Investigación y Desarrollo de Proyectos), E.T.S. de Ingenieros de Caminos, Canales y Puertos, Av./Los Castros 44, 39005 Santander, Spain.
* Corresponding author: carlos.thomas@unican.es

Abstract: The design of concrete often requires numerous mix proportions and tentative mixings, which translates into a great number of specimens and tests. The process may be optimized by using small-scale specimens, which results in the saving of material, equipment and time, offering advantages such as better handling, easy kneading or smaller curing spaces. Nevertheless, the ability of small-scale specimens to reproduce the experimental properties determined through conventional samples is an open issue. The hypothesis of this study is that the differences between standard and small-scale specimens may be mitigated by applying a change of scale to the aggregates. The durability of high-density concrete for radiation shielding, in terms of weathering resistance and behaviour against heating cycles, has been determined by means of conventional and small-scale specimens (including scaled aggregates). The effects of various aggressive external agents (heating cycles, seawater and water with K_2SO_4) and the correlation between the results from scaled and standard specimens were determined. The analysis of the results enabled to establish the suitability of the use of micro-concretes to characterize concretes. In this study, the correlations between scaled and non-scaled models have been obtained in properties such as compressive strength, mass variation and ultrasonic pulse velocity after undergoing durability and thermal exposition tests.

Keywords: Micro-concrete; high-density concrete; thermal effects; weathering; mechanical properties; durability.

1 Introduction

The study of the mechanical behaviour of concrete has traditionally been based on tests conducted on standard specimens, extrapolating the results to real-scale structures. Despite the increasingly widespread use of numerical methods in structural analysis, concrete requires -due to its intrinsic heterogeneity- a large number of tests to address structural integrity assessments.

The complexity of scaling the properties of concrete from samples to structures not only lies in the dimensional changes but also in the size of the aggregates and in the influence of the manufacturing process and the curing conditions. This effect is referred to as 'size effect'. Given the difficulties that arise in modelling the combined influence of all these factors on the final properties (mechanical, physical, etc.) of concrete, scientists have opted in many instances for establishing empirical correlations between specimens with different sizes. The size effect was already reported in the 1960s by Johnson [1], who proved that the strength of concrete increases when the scale of the specimens is reduced. Some of the following were pointed out by Noor [2]

to explain the causes behind the differences between results obtained from different scale specimens: the compaction process cannot be scaled, the higher water loss inside moulds and mixers, the increase in specific surface of the aggregates which is higher than the increase of cement paste volume and the difficulty in obtaining flat faces to apply the strength in mechanical tests. Another factor to keep in mind is the testing equipment.

The size effect may be due to material properties not properly scaled [3]. In this sense, the role played by the presence of a distribution of microcracks of different sizes randomly distributed in the material has been explained on a statistical basis [4]. The weakest link theory, developed by Weibull [5], establishes an analogy with a chain: a chain is as strong as its weakest link; therefore, the larger the test sample, the more likely its fracture becomes, because of the increased probability of finding a critical crack. However, this theory has been discarded by studies that applied it to solve the size effect when nonlinear deformations and stress redistributions are not important in the failure [6]. From a deterministic point of view, fracture occurs in a restricted region of the material where cement paste behaves plastically. For small specimens, this fracture zone is larger and the material releases more energy during fracture. For large specimens, linear elastic fracture mechanics predominates. The main precursor of this size effect theory was Bažant with its size-effect law, who establishes size effects on tensile strength and postulated a method for large specimens [7]. Kim and Yi adapted this law for compressive strength [8] also justified by Tae [9]. According to these theories, the size effect depends on the characteristic length of the specimen, the maximum aggregate size, a number of empirical constants of the material and the tensile or compressive strength, as explained above.

There are many studies on the size effect with non-proportional scaling [10] using samples with different shapes where cubes and cylinders were compared [11]. Some authors have obtained empirical conversion factors between concrete specimens with different size and shape. Some of the most used correlations were proposed by Neville [12] and Zhu and Yang [13] to translate the strength from prisms and cylinders to standardized 15 cm cubic samples. The Spanish standard for concrete design establishes a series of correlations depending on the strength and geometry of the specimens [14]. In addition, numerous studies have employed numerical simulation to determine the crack propagation path as well as the crack rate [15–17].

High temperature negatively affects the physical-mechanical properties of concrete due to dehydration, leading to the appearance of cracks [18–20]. At 120°C, unbound water is completely lost and bound water in C-S-H begins to evaporate [21]. A point of marked loss of strength occurs in the range of 400-800°C, where the complete dehydration of C-S-H gel takes place, losing its cementing capacity [22]. In addition, the degradation of portlandite ($Ca(OH)_2$) occurs at 400-500°C [23]. Under these conditions, the cement paste shrinks and the aggregates expands, generating micro-cracks, opening pores and thus affecting the mechanical performance of concrete [24]. This porous concrete becomes extremely sensitive to external agents; besides, high temperature considerably increases [25,26] the diffusion rate of chlorides (between 150% and 200% from 20°C to 45°C).

Sulphate attack typically occurs after the exposure of concrete to ground water or sulphate-containing soils. Reactions occur between the calcium hydroxide present in the cement and the sulphate ions to form gypsum and between calcium aluminate and sulphate ions to form ettringite. Another possible reaction is the formation of thaumasite, a product formed from sulphate and carbonate ions (from limestone and atmospheric carbonation) at low temperature (5°C) [27]. A number of studies have focused on the effect of different types of sulphate solutions on conventional [28] and recycled aggregate concrete, in order to analyse its durability [29], verifying the same filling and expanding process in both cases [30]. The effect of sulphates on structures subjected to bending is higher if 40% of the maximum flexural strength is exceeded [31].

In the marine environment or in tidal zones, the chlorides may reduce the lifespan and accelerate the deterioration of structures. The presence of a ferrous aggregate may accentuate the process. The combined chlorides react with the tricalcium aluminate to form Friedel's salt [32], while the free chlorides, after penetrating the concrete, react with the reinforcements, oxidizing them. Chloride transport in concrete is an advective-diffusive phenomenon that depends on the porosity of the medium, the saturation of pores, the concentration of ions in the solution and the tortuosity of the pore structure [33]. Lu [34] established the mechanisms through which the concrete's durability depends on the mix ratio, the existence of humidity-drying periods and the exposure time. Ye [35] performed an analysis of chloride ions transport models in cracks, establishing a strong dependence on crack width and roughness, capillarity, tortuosity and pore structure. In cycles that incorporate both chloride and sulphate solutions, the effect of chlorides is less corrosive on Portland cement than with chlorides alone, since sulphates retard chloride access [36].

This study is aimed at analysing weathering and temperature effects in high-density concrete for radiological shielding. Standard test specimens (high-density concrete, HDC) and small-scale cylinders (micro high-density concrete, μHDC) were compared. The main hypothesis is that size effect may be mitigated by applying the overall change of scale to the aggregates; this method would make it possible to reach independency between the scale of the specimen and its compressive strength [37]. When reducing the size of the aggregates, their specific surface increases proportionally to the overall change of scale. Consequently, the thermal response of concretes with aggregates of different scale (even if the mass proportions remain constant) will differ when subjected to thermal transient conditions. This issue is of great concern, since high-temperature conditions are prevalent in concretes for radiological shielding. To the best of these authors' knowledge, no previous research has been developed in which high-density concrete for radiological shielding was scaled using micro-concrete. Tests have been carried out in this study to determine the mechanical properties and accelerated aging by exposure to aggressive environments. Therefore, validating the use of micro-concrete for the characterization of radiological protection concretes shows two advantages. On the one hand, it supposes an important saving of material and, on the other hand, it allows results to be obtained from simplified means: less force for the determination of the mechanical properties and less intensity of the radiological sources for its characterization. The remainder of the paper is organized as follows: in section 2, the reader will find the procedure followed to scale the concrete and the corresponding mixing methods. Likewise, the aging methods and thermal shock treatments, simulating the exposure to extreme radiological conditions are described. Results are introduced in section 3 and analysed in section 4; finally, section 5 summarizes the main conclusions of the study.

2 Materials and methods

To facilitate the reading of this section, Table 1 shows a summary of the experimental methods employed.

Table 1. *Summary of experimental methodology.*

Test	Description	Specimens
Cement composition	Cement chemical composition by XRF	Dry cement powder.
Aggregate grading	Grading size of different aggregates	Sand and coarse aggregate (0/2, 0/8 and 0/20 mm).
Physical properties	Concrete and micro-concrete density, porosity and absorption	Cylinders of 10x20 cm and 2x4 cm.

Test	Description	Specimens
Heating cycles	Exposure of the concrete to high temperatures	Cubic of 10 cm and 2x4 cm Cylinders.
Mechanical properties	Compressive strength and elastic modulus of concrete and micro-concrete	Cubic of 10 cm, 10x20 cm and 2x4 cm Cylinders.
Accelerated ageing	Accelerated ageing by cycles into salt solutions	Cylinders of 10x20 cm and 2x4 cm.
Mass variation	Accelerated ageing effects by loss of specimen mass	Cylinders of 10x20 cm and 2x4 cm.
Ultrasonic pulse velocity	Accelerated aging effects by ultrasonic pulse velocity	Cylinders of 10x20 cm and 2x4 cm.

2.1. Materials and mix proportions

Magnetite aggregates have been used due to their radiological shielding ability to manufacture HDC and μHDC specimens. The magnetite natural aggregates are separated in three sizes, fine (AF: 0/2 mm), medium (AM: 0/8 mm) and coarse aggregates (AC: 0/20 mm), respectively. The aggregate contains more than 90% wt. of magnetite, according to the supplier, having a density of 5.15 g/cm^3 in the case of AF and 4.77 g/cm^3 for AM and AC, according to EN 1097-6 [38]. The average iron content is 43% wt. determined by Energy Dispersive X-ray spectroscopy . Unscaled concrete incorporates AM and AC while scaled concrete incorporates AF and AM. The aggregate size-grading curves are shown in Fig. 1.

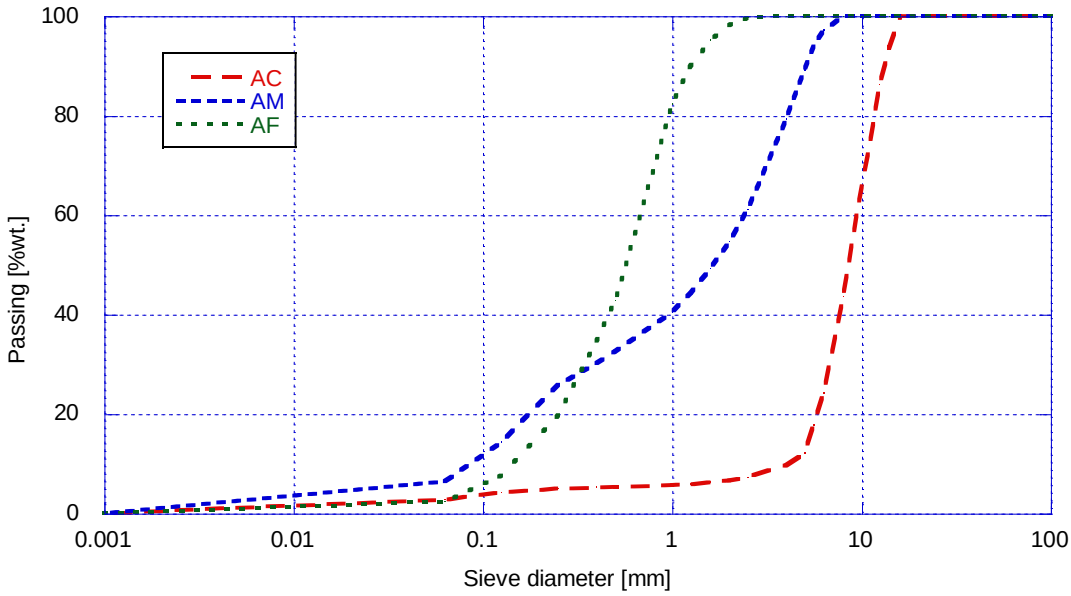

Fig. 1. *Experimental curves obtained after grading the different aggregate sizes, AC, AM and AF.*

Superplasticizer (SP) additive has been used for the HDC and μHDC, as well as Portland cement CEM I 52.5N with a specific Blaine surface area of 443.1 m^2/kg, determined following the standard EN 196-6 [39]. The mix proportions used for HDC have been determined through the Fuller method, obtaining a water/cement ratio of 0.59 and a 1.3% additive/cement rate. The chemistry (oxides-composition) of the cement has been obtained by X-Ray fluorescence (XRF) and the results obtained are shown in Table 2.

Table 2. *Cement chemical composition by XRF.*

Cement	CaO	SiO_2	Al_2O_3	Fe_2O_3	SO_3	K_2O	MgO	TiO_2	C
CEM I 52.5 N/SR	68.5	18.44	3.12	2.68	3.21	0.54	1.16	0.17	0.46

The design of micro-concrete is based on incorporating aggregates that maintain the same dimensional proportions as those of the aggregates in the unscaled concrete. The aggregate with scaled grading (AS) is a modification of the AF fraction incorporating fines of the AM fraction and from which the thickest fractions are extracted to obtain a grading curve equivalent to the aggregate grading of the unscaled concrete. To determine the amount of material to be added or extracted, the relationship between the maximum size of the scaled and unscaled concrete ($D^{max}_{unscaled}/D^{max}_{scaled}$) was obtained. This ratio must be equal to 7.5, which is the size factor between the small-scale (2x4 cm) and the standard (15x30 cm) cylindrical specimens. Accordingly, since $D^{max}_{unscaled}$ is 20 mm, D^{max}_{scaled} must be 2.67 mm. The fraction of the nearest American Standard Sieve Series is 2.8 mm, so the D^{max}_{scaled} corresponds to the maximum size of the AF, and the $D^{max}_{unscaled}/D^{max}_{scaled}$ ratio (20 mm/2.8 mm) is ~7. This factor is applied to the other fractions of the unscaled set, obtaining a scaled size grading (SG) which is shown in Fig. 2. The graph shows the mix proportion of the scaled aggregate (AS) after the mixing to verify the size distribution of SG. The mixing has been carried out by a riffle type sample splitter. The mix proportions of the μHDC are proportional to HDC, as reflected in 0.

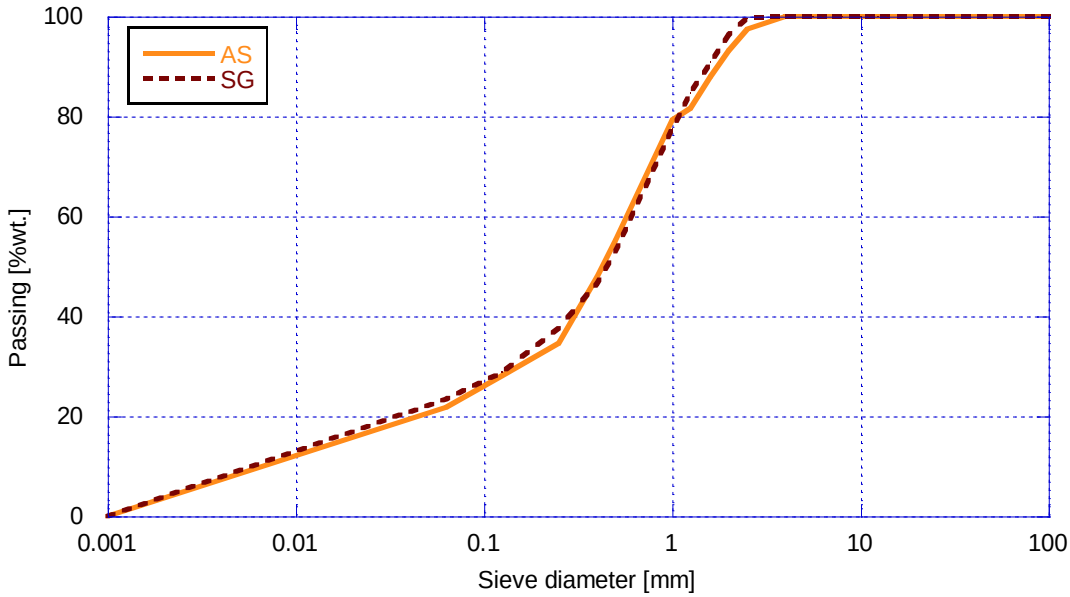

Fig. 2. *Mix aggregates size grading for μHDC.*

For the preparation of HDC, a concrete mixer with vertical axis and a capacity of 50 l was used. The mixing is divided into three phases: (i) 3 min of kneading with aggregates, cement and water, (ii) 3 min of rest and (iii) 2 min of mixing with the additive. The compaction of the specimens was carried out in two steps with a vibrating needle; the specimens were demoulded after 24 h and submerged in water for 28 days at 20 ± 2 °C.

Table 3. *Unscaled and scaled concrete mix proportions.*

Compound	Weight [kg/m³]		Volume [l/m³]	
	HDC	μHDC	HDC	μHDC
CEM I 52.5N	300	300	100	100
Water	176	176	176	176
AM	2494	0	524	0
AC	935	0	196	0
AS	0	3715	0	720
SP	4	4	4	4
TOTAL	3910	4190	1000	1000

The internal diameter and length of the moulds used for μHDC are 2 cm and 5 cm, respectively. The mixing was conducted according to the standard EN-196-1 [40] on methods for cements testing, using a mortar mixer. The mixing is divided into 5 phases: (i) 30 s water + cement at low speed, (ii) 30 s with aggregate added at low speed, (iii) 30 s of mixing at high speed, (iv) 90 s. resting and (v) 60 s mixing at high speed. The pouring in moulds is performed in two steps, at the end of each of which vibration compaction is carried out on a mortar flow table. After filling, the moulds were covered with a wet cloth to prevent moisture loss and were demoulded 24 h after manufacture. In the curing process, the μHDC specimens remained immersed in water at 20 ± 2 °C for 28 days. After 28 days, the specimens were polished on their upper and lower faces to avoid edge effects introduced by the vibration and the aggregates. Once cured, both types of test specimens were dried in an oven to constant weight before testing.

2.2. Physical properties

The physical properties have been determined on five HDC and five μHDC specimens after curing for 28 days. The bulk specific gravity, apparent specific gravity and bulk saturated surface dry specific gravity were obtained following EN 12390-7 [41]. The water absorption coefficient (%wt.) and the porosity (%vol.) were determined according to the standard UNE 83980 [42].

2.3. Heating cycles

Thermal cycles were applied on three HDC and three μHDC specimens aged 28 days for each of the five target temperatures: 100, 300, 500, 700 and 1000°C. Specimens were heated in a muffle furnace at a heating rate of 7°C/min. These heating rates are established to check the effects of severe heating conditions. They remained 30 min at this temperature and then they were cooled inside the furnace up to room temperature (20 ± 2°C). The heating/cooling curves are shown in Fig. 3.

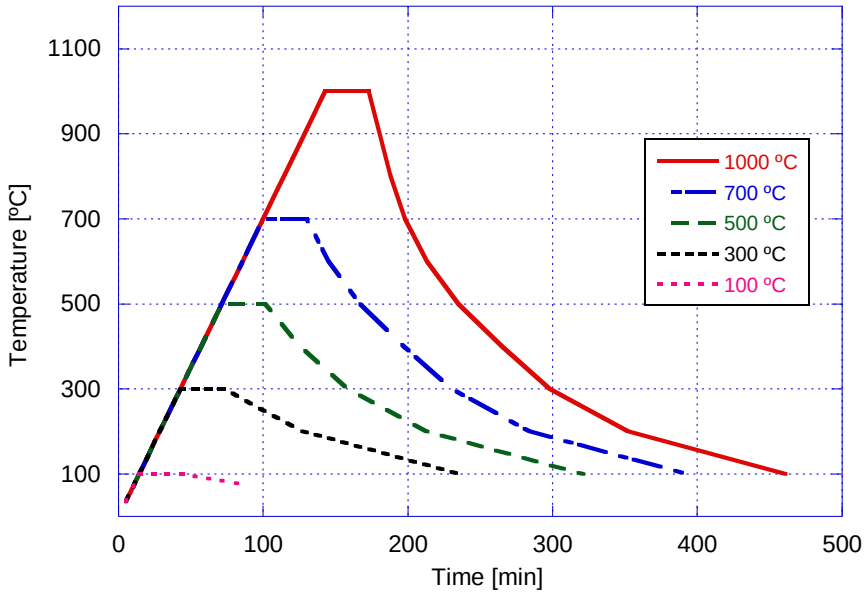

Fig. 3. *Heating cycles to which HDC and μHDC specimens were subjected.*

2.3.1. Ultrasonic pulse velocity test after heating cycles

The ultrasonic pulse velocity test was carried out on the 30 specimens (three HDC and three μHDC specimen x five temperatures), previously subjected to heating cycles. The tests have been performed before the uniaxial compressive test in direct transmission, according to EN 12504-4 [43]. The ultrasonic pulse velocity (v) is calculated as the ratio between the length of the specimen (l) and the travel time (t), as shown in Eq. (1):

$$v = \frac{l}{t}\ [km/s] \tag{1}$$

2.3.2. Compressive strength after heating cycles

The compressive tests were carried out on the 30 specimens previously subjected to heating cycles (three HDC and three μHDC specimen x five temperatures). The specimens were tested at 28 days of age, right after tempering at room temperature (20 ± 2°C). The specimens have been tested in a servo-hydraulic press with a loading capacity of 2000 kN, following EN 12390 – 3 [44].

2.4. Accelerated aging

Accelerated aging, in terms of drying-wetting cycles, was carried out on five HDC and five μHDC specimens under two different environments: seawater and water with K_2SO_4 (mineral inorganic fertilizer) at 5% wt. The experimental methodology consists of 15 drying cycles of 16 h in an oven at 105°C (the standard temperature for drying concrete specimens) and 15 humidity cycles of 8 h in which the samples remain submerged in their corresponding solution at 20 ± 2°C. The total duration of the cycles is 15 days. The first cycle begins with the test specimens completely dried.

2.4.1. *Compressive strength after accelerated aging*

The compressive tests were carried out on the 20 specimens previously subjected to drying-wetting cycles (five HDC and five μHDC specimen x two environments). The specimens were tested at 43 days of age (28 days of curing + 15 days of drying-wetting cycles). Times are identical for both HDC and μHDC. The testing methodology is the same as that explained in section 2.3.1.

2.4.2. *Mass variation*

The weight of the 20 specimens subjected to accelerated aging was measured after each drying-wetting cycle. After each drying cycle, the test specimens were cooled to room temperature before being weighted. After each wetting cycle, the test specimens were dried superficially with a wet cloth, to obtain the saturated surface dry (SSD) weight. The evolution of the dry and saturated weights (w_c) was obtained through the series of measurements and was expressed in terms of the relative weight variation (w_{rel}) to the first dry and saturated weights (w_i), respectively, according to Eq. (2). The mass gain/loss trend was determined from these values.

$$\boldsymbol{w_{rel}} = \frac{\boldsymbol{w_c - w_i}}{\boldsymbol{w_i}}\ [\boldsymbol{g/g}] \tag{2}$$

2.4.3. *Ultrasonic pulse velocity test during accelerated aging*

This method was conducted on 10 specimens (five μHDC specimen x two environments) subjected to drying-wetting cycles. The tests have been carried out after each drying and wetting cycle, in direct transmission, as explained in section 2.3.2.

3 Results

3.1. *Physical properties*

Table 4 shows the physical properties of the HDC and μHDC.

Table 4. *Physical properties of the HDC and μHDC.*

Specimen	Apparent specific gravity [g/cm³]	Bulk specific gravity [g/cm³]	Bulk SSD specific gravity [g/cm³]	Open Porosity [% vol.]	Water absorption [% wt.]
HDC	3.8	4.3	3.97	9.8	2.53
μHDC	3.71	4.43	3.88	16.2	4.36

3.2. *Heating cycles*

3.2.1. *Ultrasonic pulse velocity test after heating cycles*

Fig. 4 (left) shows the evolution of the ultrasonic pulse velocity for the different heating cycles and for both types of specimens, HDC and μHDC. Fig. 4 (right) shows the correlation between both specimens.

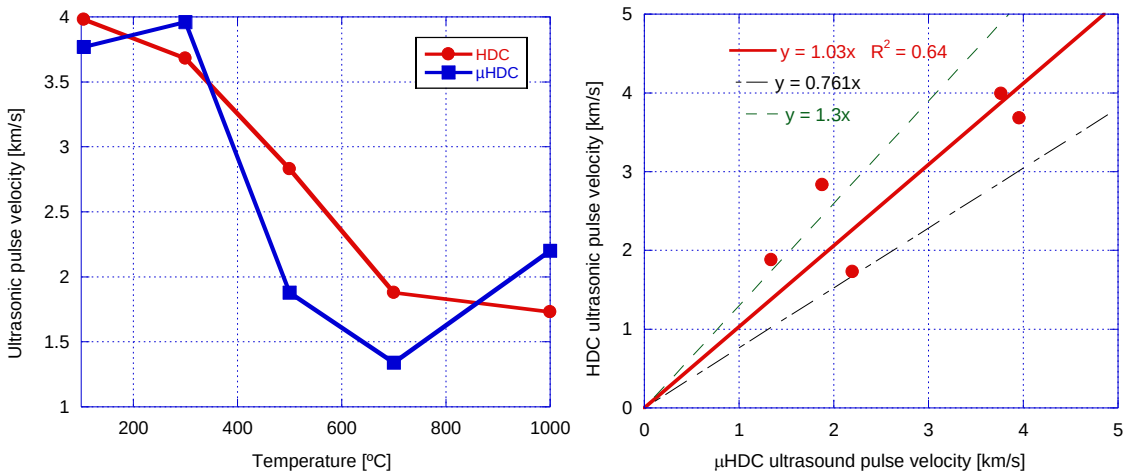

Fig. 4. *Ultrasonic pulse velocity for HDC and µHDC after undergoing heating cycles (left) and correlation (right).*

3.2.2. Compressive strength after thermal cycles

¡Error! No se encuentra el origen de la referencia. (left) shows the evolution of the compressive strength after subjecting the unscaled and scaled specimens to heating cycles and **¡Error! No se encuentra el origen de la referencia.** (right) shows the relationship between HDC and µHDC specimens.

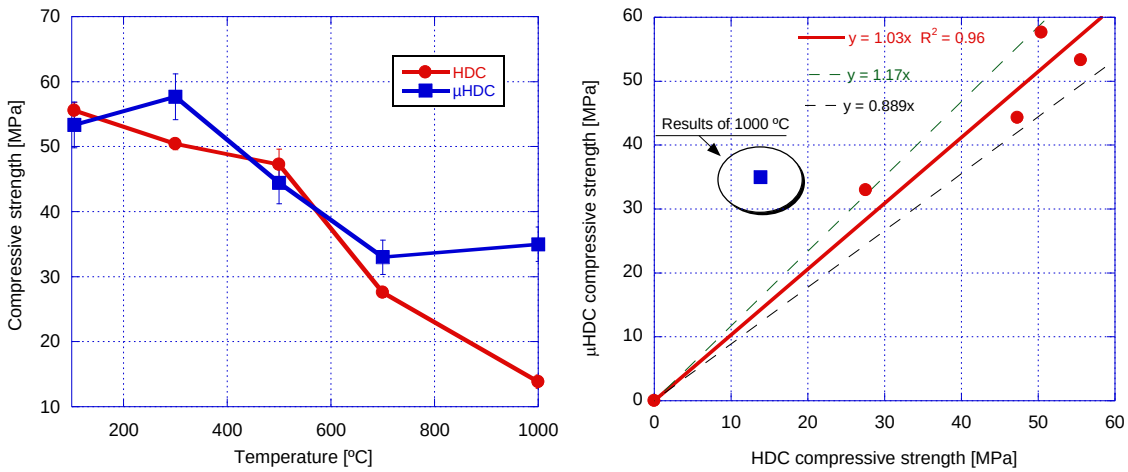

Fig. 5. *Compressive strength for HDC and µHDC as a function of temperature during heating cycles (left); correlation between the strength of HDC and µHDC (right).*

3.3. Accelerated aging

3.3.1. Compressive strength after accelerated aging

Table 5 shows the results obtained from the compressive tests after exposing the samples to drying-wetting cycles.

Table 5. *HDC and µHDC compressive strength [MPa] after drying-wetting cycles.*

Concrete:	HDC	µHDC
Control	47.05	52.36
Sea water	46.15	73.14
Sulphates	46.58	70.18

3.3.2. Mass variation

Fig. 6 (left) shows the mass variation of unscaled and scaled specimens subjected to drying-wetting cycles in seawater and Fig. 6 (right) shows the evolution of mass on µHDC and HDC specimens subjected to drying-wetting cycles in a 5% wt. K_2SO_4 solution. In Fig. 7 the correlation between both types of specimens is shown, both for seawater and for sulphates solution.

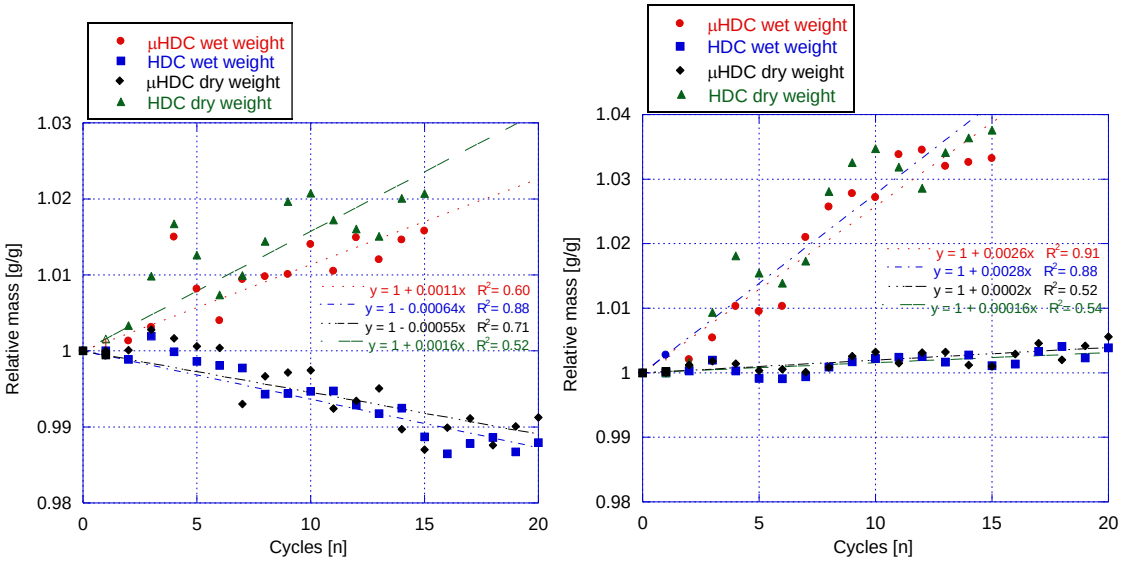

Fig. 6. *Mass variation under wetting-drying cycles in seawater (left) and sulphates (right).*

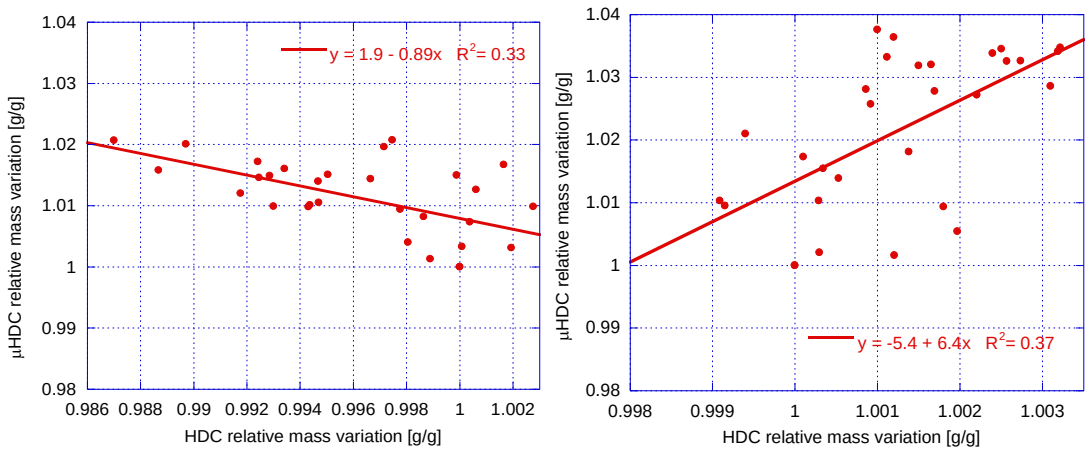

Fig. 7. Mass correlation between scaled and unscaled specimens for seawater (left) and sulphates (right) cycles.

3.3.3. *Ultrasonic pulse velocity test during accelerated aging*

Fig. 8 shows the evolution of the ultrasonic pulse velocity through the specimens subjected to drying-wetting cycles in the two aggressive solutions for μHDC.

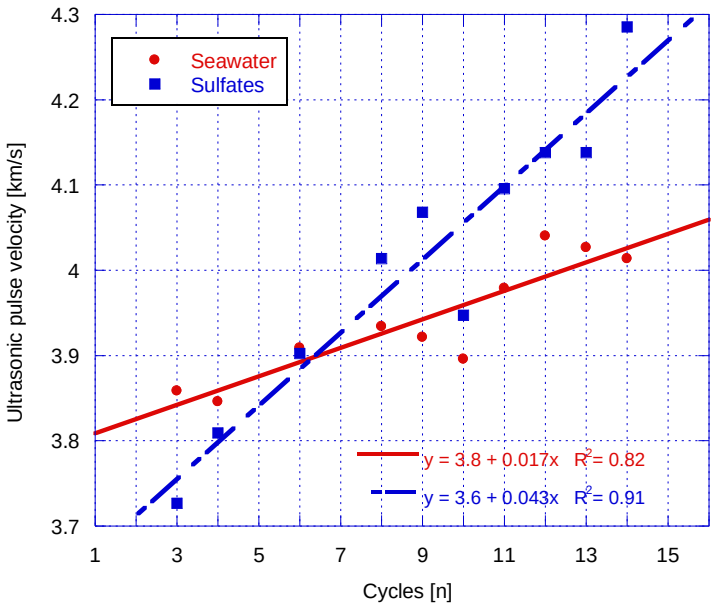

Fig. 8. *Ultrasonic pulse velocity for μHDC after drying/wetting cycles.*

4 Discussion

4.1. *Physical properties*

Both types of specimens have high apparent density (Table 4), close to 4 g/cm^3, which makes them appropriate to be used in structural elements for gamma radiation shielding. The specific gravities are similar for both types of concrete. Water absorption is low compared to porosity due to the high density of the concrete.

The most noticeable difference between the two specimens lies in the porosity: while HDC has a porosity close to 10%, in μHDC this value rises to 16%. The same effect occurs for water absorption; whose value depends on the volume of accessible pores. This is due to the larger amount of filler particles below 64 μm in μHDC than in HDC and the consequent increase in the specific surface of the aggregates. In addition, it is easier to saturate internal pores in μHDC than in HDC, due to the seven times higher specific surface of the former.

4.2. *Heating cycles*

4.2.1. *Compressive strength after thermal cycles*

Both types of specimens show a progressive loss of strength with rising temperature (Fig. 4 left). HDC specimens lost 15% of the initial strength for a temperature of 300°C; then, a strong process of continuous loss of strength occurs until the final temperature of 1000°C. After heating cycles, microcracks appeared in the material due to the different expansion coefficients of aggregates and paste, the drying of the C-S-H gel and the decomposition of hydration products

such as portlandite; all these processes reduced the residual compressive strength of concrete by 75% at 1000 °C.

The μHDC specimens show a slightly different behaviour. In the range between 100 and 300°C, compressive strength increased by almost 8%, a phenomenon previously reported in conventional concretes [45,46] which is a result of the late hydration of the non-hydrated cement grains due to the circulation of water vapour [47]. This type of hydration appears to be more likely in μHDC than in HDC because of the shorter moisture migration paths and higher porosity. μHDC lost 45% of its strength between 300 and 700°C. Between 700 and 1000°C strength slightly increases because of the sintering mechanisms that occur preferentially in μHDC due to its lower grain size [48].

Comparing the two types of specimens, **¡Error! No se encuentra el origen de la referencia.** (left), a slight size-effect still remains, despite the use of scaled aggregates [1]. For exposure temperatures lower than 700°C, an experimental average scale factor of 0.95 can be established (this factor may depend on strength [49]. **¡Error! No se encuentra el origen de la referencia.** (right) shows a strong linear relationship between the strength of HDC and μHDC.

The concretes, both standard and scaled, show a very similar behaviour up to 800°C, **¡Error! No se encuentra el origen de la referencia.** (right). The obtained values can be related according to:

$$\boldsymbol{f} = \frac{\mathbf{f'-0.045}}{\mathbf{0.91}} \tag{3}$$

where f is the compressive strength of standard specimens and f' is the compressive strength of the scaled specimens. However, concretes subjected to 1000°C show different behaviours. The test specimens of different size are affected in different way after exposure to high temperatures. The observed differences are accentuated at 1000°C because the exposure temperature has affected more the smaller test specimens. High temperature causes an increase in the compressive strength due to a more resistant structure as consequence of the sintering of the magnetite (~1000°C)[48].

4.2.2. Ultrasonic pulse velocity test after heating cycles

Both types of specimens Fig. 4 (left) show a similar trend but the changes for μHDC are more pronounced. These differences in pulse velocity suggest the existence of slight size effects. HDC specimens suffer lower variability because heating affects its voluminous structure to a lower degree, a fact that confers greater thermal inertia and stability against thermal intensities of equal magnitude. In the curve for μHDC, two regions of velocity increase are shown; the first one takes place between 100°C and 300°C and corresponds to the late hydration of cement, explained before; the second zone corresponds to the sintering of the magnetite (~1000°C) characterized by an increase in grain size and material compactness [48]. The differences in pulse velocity observed at 500°C are presumably a consequence of different levels of decomposition of hydration products, that take place earlier at smaller specimens, μHDC. Fig. 4 (right) shows a relatively high correlation between the two scaled specimens.

4.3. Accelerated aging

4.3.1. Compressive strength after accelerated aging

The control specimens (untreated), which have remained in the furnace at 100°C during the durability cycles, show a 10% higher strength for μHDC (Table 5). The immersion in salt solution

for HDC specimens has little impact on their strength, which is reduced by around 2% -for seawater-, a negligible variation, previously obtained by other authors after months of immersion [50,51]. The aging on the μHDC increases the concrete strength due to a late hydration process favoured by the presence of water. The salts have not yet interacted with the paste and the crystallization of the salts in solution within the pores may have increased the pressure in the pores according to the mechanism explained by Flatt [52]. This expansive pressure opposes the compressive forces on the samples during the test.

The specimens subjected to drying-wetting cycles in seawater after heating cycles from 100 to 1000°C (105°C is the same temperature as in the drying cycles) show a particular behaviour when compared to the heating cycle effects of section 3.2. At 100°C, the specimens slightly increase their strength, because at 43 days of age (28 + 15 for cycles) a larger number of cement grains have been hydrated. After a visual analysis Thomas et al. [53] found that concrete does not show any signs of deterioration or degradation after wet–dry cycles or wetting–drying cycles to 105 ºC. At 300°C, a slight strength increase is obtained and, at 500 and 700°C, a large loss due to the decomposition of the C-S-H gel.

4.3.2. Mass variation

Fig. 6(left) shows the mass variation of unscaled and scaled specimens subjected to drying-wetting cycles in seawater. For μHDC, there is a relatively high mass increase in cycle 15 of around 1.5% wt. for the dry and wet weights. In both cases, linear fittings were used to model the evolution of mass variation. Some authors [50] consider that this mass gain in the paste is associated with capillarity absorption of water during the cement hydration accompanied by the change in the concrete structure over time. This hydration generates more C-S-H, which has a large specific surface and absorbs more water. The increase in mass may also be due to the precipitation of salt both on the surface of the specimen and in the pores [51], whose effect will be greater in μHDC than in HDC specimens since they have a higher specific surface. This effect of mass gain should end when the test piece becomes saturated. A scanning electron micrograph of one of these specimens after the ageing process is shown in Fig. 9.

In contrast, HDC samples show a loss of mass of around 1% wt. in cycle 15 for the dry and wet weights. This slight variation, which was modelled through a linear fitting, may be due to the material detached from the specimen, as is shown in Fig. 6 (left). HDC specimens cannot absorb as much fluid as the micro-concretes because the immersion time is the same and pore paths are much longer, so the salt assimilation will be much smaller. As in micro-concretes, the dry weight shows a variation similar to that of the wet weight throughout the cycles, although in the comparison between both specimens, the total variation is higher in micro-concretes, as would be expected.

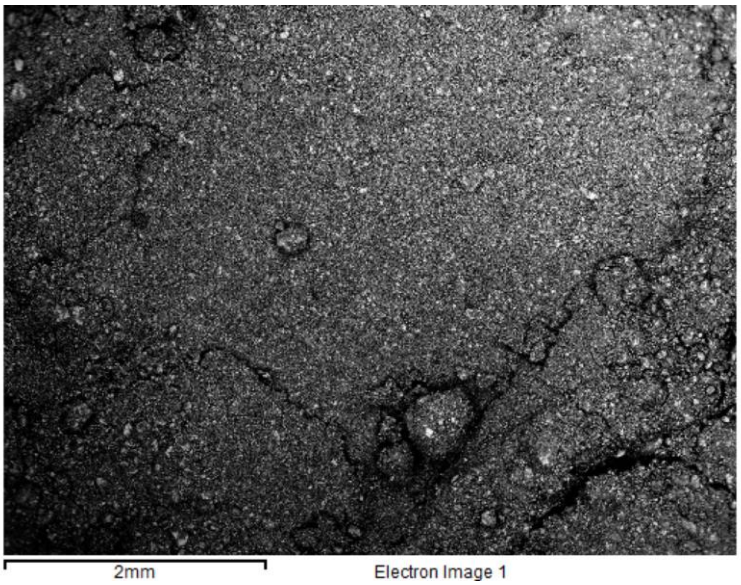

Fig. 9. *Scan electron micrograph of the surface of a μHDC after aging.*

μHDC specimens in K_2SO_4 solution (Fig. 6)display a very significant mass gain of ~4% wt. in cycle 15 for the dry and wet weights is observed. This gain, which had already been reported previously [50] is also appreciated to a lower degree, 0.4% wt., in HDC specimens; the effect is less pronounced since HDC samples have smaller specific surface area and larger pore structure. This mass increase can be explained analogously to the argument exposed previously, based on the larger amount of salt precipitated. This precipitation may be greater because of the interactions between the sulphate ions and the paste, producing a lower cohesion among the products of the cement hydration, expansive gypsum and ettringite [54] that generate a greater circulation surface and therefore greater deposition for the chloride solution. In Fig. 7 the correlation between both types of specimens is shown, both for seawater and for sulphates solution, obtaining a moderate correlation [55] in any case.

In summary, for both exposure environments, it is observed that the dry weight shows a greater initial variation. This is because the first dry weight has been made with the specimens completely dry. Also, for both types of specimens, a greater mass increase in sulphates than in chlorides can be observed and this increase is greater in scaled specimens because more specific surface implies that the particles of salts that adhere in the specimen provide more relative weight.

¡Error! No se encuentra el origen de la referencia. shows the evolution of the dry mass for the test specimens that have been subjected to heating cycles before undergoing drying-wetting cycles. The trend for all the tested temperatures is a gain of mass from 1% to 3.5% to cycle 13. As the temperature to which the specimen has been subjected increases, the mass gain is greater. This is due to the volumetric expansion produced by heat, the degradation of the paste due to the dehydration of the hydration products, and to the flaws and discontinuities propitiated by both causes, which allow a greater quantity of solution to penetrate and deposit in the pores. The specimens subjected to the highest temperature do not follow the previous rationale, since upon reaching the sintering temperatures of the magnetite (1000-1100 °C) the mineral grains have partially melted, increasing the shrinkage and reducing the concrete porosity significantly [48].

4.3.3. Ultrasonic pulse velocity test during accelerated aging

Both in sulphate and seawater solutions, a linear velocity increase is observed during the first 15 cycles, increasing by 5% and 10% correspondingly (Fig. 8). This increase is due to the fact that the concrete continues being hydrated within the testing solution, as has already been justified by Tsivilis [56], who obtains gains in the ultrasonic pulse velocity up to a month and a half after the beginning of the solution exposition. This gain is directly related to the gain of mass through the cycles. This is demonstrated by the fact that the weight experienced a gain of 2% in the case of seawater and 3.5% in the case of sulphate dissolution. It is observed that this mass increase is proportional to the pulse velocity increase, higher in the case of sulphates due to a greater salt precipitation in the porous surface of the specimens. On the other hand, the mass loss effect caused by the interactions between the salt and the matrix is still inappreciable because the process is still in its early stages.

Fig. 8 (right) shows how temperature affects the concrete durability, A generalized tendency of the increase in the pulse velocity is observed, but this gain level and the velocity values in the first cycle, depend on the exposure temperature of the specimen. In cycle 1, it is verified how the temperature negatively affects the pulse velocity, as already explained at the beginning of the section. The running of the cycles leads to an additional hydration of the binder but also to a mass increase propitiated by the salt deposition on the surface of the specimens. Both arguments justify an increase in the pulse velocity, but this increase is greater in specimens subjected to higher temperatures because the initial level of micro-cracks and discontinuities (and consequently the saturation of the pores with salt crystals over the cycles) is larger. The propagation velocity of all the specimens tends to become equal; this equalization shows the relation of this property with the durability of any concrete.

5 Conclusions

High-density concretes for radiological shielding show singularities. There is little previous research to analyse the effect of high temperatures on their durability. This research provides relevant information regarding this point. It has been demonstrated that these concretes can be characterized using scaled specimens up to certain temperatures. From the analysis of the results obtained, the following conclusions and recommendations can be drawn:

Scaled and unscaled specimens have a similar bulk specific gravity, but the micro-concretes show an absolute porosity 6% higher due to having a less homogeneous fines fraction.

The compressive strength of both types of specimen significantly decreases with the increase in temperature, although the micro-concretes show a greater absolute resistance, and a greater loss with the increase in temperature due to their lower thermal inertia. Sintering reactions are easier to reach in micro-concretes, increasing their compactness and strength at 1000°C.

The mass variation in drying/wetting cycles is greater in micro-concretes since they have shorter migration paths and higher porosity, which facilitates a greater salt deposition rate. Exposure to high temperatures generates more discontinuities, accentuating this behaviour.

The ultrasonic pulse velocity reduces with the temperature and this decrease is more accentuated in micro-concretes in an analogous behaviour to compressive strength. As a greater number of drying-wetting cycles is reached, the ultrasonic pulse velocity increases, and tends to equalize for all exposition temperatures, due to the saturation of salts in the pores.

Relatively high correlation levels have been found for micro-concretes and unscaled specimens in compressive strength and ultrasonic pulse velocity after exposure to high temperatures, while correlation values for the mass variation after drying-wetting cycles are relatively poor.

Acknowledgments

This research was developed at LADICIM (Laboratory of Materials Science and Engineering Division) of the University of Cantabria in collaboration with the company INGECID, under the financial supports of the European Regional Development Fund (ERDF) and the Ministry of Economy, Industry and Competitiveness (MINECO).

Conflict of Interest Statement

Funding: This study was funded by the *Ministerio de Economía y Competitividad* (ES), research project RTC-2016-5637-3, and Pablo Tamayo was hired at this researcher project during the study. The authors declare that they have no other conflict of interest.

References

[1] Johnson RP. Strength tests on scaled-down concretes suitable for models, with a note on mix design. Mag Concr Res 1962;14:47–53.

[2] Cunningham CH, Townsend FC, Fagundo FE. No Title. Dev Micro-Concrete Scale Model Test Buried Struct 1986.

[3] Laefer DF, Erkal A. Selection, production, and testing of scaled reinforced concrete models and their components. Constr Build Mater 2016;126:398–409. doi:https://doi.org/10.1016/j.conbuildmat.2016.08.129.

[4] Bazant ZP, Chen E-P. Scaling of structural failure. Appl Mech Rev 1997;50:593–627.

[5] Weibull W. A statistical theory of the strength of materials. IngVetAkHandl 1939.

[6] Van Vliet MRA, Van Mier JGM. Experimental investigation of size effect in concrete and sandstone under uniaxial tension. Eng Fract Mech 2000;65:165–88.

[7] Bažant ZP. Size effect on structural strength: a review. Arch Appl Mech 1999;69:703–25.

[8] Kim J-K, Yi S-T. Application of size effect to compressive strength of concrete members. Sadhana 2002;27:467.

[9] Yi S-T, Yang E-I, Choi J-C. Effect of specimen sizes, specimen shapes, and placement directions on compressive strength of concrete. Nucl Eng Des 2006;236:115–27.

[10] Lei W-S, Yu Z. A statistical approach to scaling size effect on strength of concrete incorporating spatial distribution of flaws. Constr Build Mater 2016;122:702–13.

[11] Del Viso JR, Carmona JR, Ruiz G. Shape and size effects on the compressive strength of high-strength concrete. Cem Concr Res 2008;38:386–95.

[12] Sabnis GM, Mirza SM. Size effect in model concretes. J Struct Div 1979;105:1007–20.

[13] ZHU E, YANG W, WANG J, LIN W. Relationship of Compressive Strength of Specimens with Various Shapes and Sizes for C20 MPa Grade Concrete. J North Jiaotong Univ 2005;1.

[14] Estructural IE del H. EHE-08. Madrid, Minist Fomento, Secr Gen Técnica 2008.

[15] Alava MJ, Nukala PKV V, Zapperi S. Fracture size effects from disordered lattice models. Int J Fract 2008;154:51.

[16] Van Mier JGM, Van Vliet MRA. Influence of microstructure of concrete on size/scale effects in tensile fracture. Eng Fract Mech 2003;70:2281–306.

[17] Ince R, Arslan A, Karihaloo BL. Lattice modelling of size effect in concrete strength. Eng Fract Mech 2003;70:2307–20.

[18] Alonso C, Andrade C, Menendez E, Gayo E. Evolucion de la microestructura de hormigones de alta y ultra resistencia al ser expuestos a ambientes de elevadas temperaturas. Hormigón y Acero 2001.

[19] Thomas C, Rico J, Tamayo P, Setién J, Ballester F, Polanco JA, et al. Neutron shielding concrete incorporating B4C and PVA fibers exposed to high temperatures. J Build Eng 2019;26:100859. doi: https://doi.org/10.1016/j.jobe.2019.100859.

[20] Thomas, C.; Rico, J.; Tamayo, P.; Balllester, F.; Setién, J.; Polanco JA. Effect of elevated temperature on the mechanical properties and microstructure of heavy-weight magnetite concrete with steel fibers. Cem Concr Compos 2019;103:80-8. doi: https://doi.org/10.1016/j.cemconcomp.2019.04.029.

[21] Lion M, Skoczylas F, Lafhaj Z, Sersar M. Experimental study on a mortar. Temperature effects on porosity and permeability. Residual properties or direct measurements under temperature. Cem Concr Res 2005;35:1937–42. doi:https://doi.org/10.1016/j.cemconres.2005.02.006.

[22] Chan YN, Peng GF, Anson M. Residual strength and pore structure of high-strength concrete and normal strength concrete after exposure to high temperatures. Cem Concr Compos 1999;21:23–7. doi:https://doi.org/10.1016/S0958-9465(98)00034-1.

[23] Lima RCA, Haesbaert FM, Caetano LF, Bergmann CP, S. FILHO LCP. Microstructural Changes in High Density Concretes Exposed to High Temperatures. Rev IBRACON Mater 2005;1.

[24] Hager I. Behaviour of cement concrete at high temperature. Bull Polish Acad Sci Tech Sci 2013;61:145–54.

[25] Jones MR, Dhir RK, Gill JP. Concrete surface treatment: effect of exposure temperature on chloride diffusion resistance. Cem Concr Res 1995;25:197–208.

[26] Al-Khaja WA. Influence of temperature, cement type and level of concrete consolidation on chloride ingress in conventional and high-strength concretes. Constr Build Mater 1997;11:9–13.

[27] Gaze ME, Crammond NJ. The formation of thaumasite in a cement:lime:sand mortar exposed to cold magnesium and potassium sulfate solutions. Cem Concr Compos 2000;22:209–22. doi:https://doi.org/10.1016/S0958-9465(00)00002-0.

[28] Jiang L, Niu D. Study of deterioration of concrete exposed to different types of sulfate solutions under drying-wetting cycles. Constr Build Mater 2016;117:88–98.

[29] Thomas C, Setién J, Polanco JA, Alaejos P, Sánchez De Juan M. Durability of recycled aggregate concrete. Constr Build Mater 2013;40:1054–65.

[30] Qi B, Gao J, Chen F, Shen D. Evaluation of the damage process of recycled aggregate concrete under sulfate attack and wetting-drying cycles. Constr Build Mater 2017;138:254–62.

[31] Gao J, Yu Z, Song L, Wang T, Wei S. Durability of concrete exposed to sulfate attack under flexural loading and drying–wetting cycles. Constr Build Mater 2013;39:33–8.

[32] Suryavanshi AK, Narayan Swamy R. Stability of Friedel's salt in carbonated concrete structural elements. Cem Concr Res 1996;26:729–41. doi:https://doi.org/10.1016/S0008-8846(96)85010-1.

[33] Maekawa K, Ishida T, Kishi T. Multi-scale modeling of concrete performance. J Adv Concr Technol 2003;1:91–126.

[34] Lu C, Gao Y, Cui Z, Liu R. Experimental analysis of chloride penetration into concrete subjected to drying–wetting cycles. J Mater Civ Eng 2015;27:4015036.

[35] Ye H, Jin N, Jin X, Fu C. Model of chloride penetration into cracked concrete subject to drying–wetting cycles. Constr Build Mater 2012;36:259–69.

[36] Chen Y, Gao J, Tang L, Li X. Resistance of concrete against combined attack of chloride and sulfate under drying–wetting cycles. Constr Build Mater 2016;106:650–8.

[37] Fládr J, Bílý P. Specimen size effect on compressive and flexural strength of high-strength fibre-reinforced concrete containing coarse aggregate. Compos Part B Eng 2018;138:77–86.

[38] 1097-6 EN. Tests for mechanical and physical properties of aggregates. Determination of particle density and water absorption n.d.

[39] 196-6 EN. Methods of testing cement - Part 6: Determination of fineness 2010.

[40] 196-1 EN. Methods of testing cement - Part 1: Determination of strength 2005.

[41] EN-12390-7. Testing hardened concrete - Part 7: Density of hardened concrete 2009.

[42] 83980 UNE. Durabilidad del Hormigón. Métodos de ensayo: Determinación de la absorción, densidad y la porosidad accesible al agua del hormigón. 2014.

[43] 12504-4 EN. Testing concrete - Part 4: Determination of ultrasonic pulse velocity 2006.

[44] 12390-3 EN. Testing hardened concrete - Part 3: Compressive strength of test specimens 2009.

[45] Arioz O. Effects of elevated temperatures on properties of concrete. Fire Saf J 2007;42:516–22. doi:https://doi.org/10.1016/j.firesaf.2007.01.003.

[46] Peng G-F, Yang W-W, Zhao J, Liu Y-F, Bian S-H, Zhao L-H. Explosive spalling and residual mechanical properties of fiber-toughened high-performance concrete subjected to high temperatures. Cem Concr Res 2006;36:723–7. doi:https://doi.org/10.1016/j.cemconres.2005.12.014.

[47] Piasta J, Sawicz Z, Rudzinski L. Changes in the structure of hardened cement paste due to high temperature. Matériaux Constr 1984;17:291–6.

[48] Forsmo SPE, Forsmo S-E, Samskog P-O, Björkman BMT. Mechanisms in oxidation and sintering of magnetite iron ore green pellets. Powder Technol 2008;183:247–59.

[49] Fomento - Gobierno de España M. EHE-08: Code on Structural Concrete 2008.

[50] Sotiriadis K, Nikolopoulou E, Tsivilis S. Sulfate resistance of limestone cement concrete exposed to combined chloride and sulfate environment at low temperature. Cem Concr Compos 2012;34:903–10.

[51] Wang K, Nelsen DE, Nixon WA. Damaging effects of deicing chemicals on concrete materials. Cem Concr Compos 2006;28:173–88.

[52] Flatt RJ. Salt damage in porous materials: how high supersaturations are generated. J Cryst Growth 2002;242:435–54. doi:https://doi.org/10.1016/S0022-0248(02)01429-X.

[53] Thomas C, Lombillo I, Polanco J a., Villegas L, Setién J, Biezma M V. Polymeric and cementitious mortars for the reconstruction of natural stone structures exposed to marine environments. Compos Part B Eng 2010;41:663–72. doi:10.1016/j.compositesb.2010.08.007.

[54] Santhanam M, Cohen MD, Olek J. Mechanism of sulfate attack: a fresh look: Part 2. Proposed mechanisms. Cem Concr Res 2003;33:341–6. doi:https://doi.org/10.1016/S0008-8846(02)00958-4.

[55] Cohen-Adad R, Hassen-Chehimi D Ben, Zayani L, Cohen-Adad M-T, Trabelsi-Ayedi M, Kbir-Ariguib N. Modelling of multicomponent salt systems: Application to sea water and brines I. Derivation of the model. Calphad 1997;21:521–34. doi:https://doi.org/10.1016/S0364-5916(98)00009-1.

[56] Tsivilis S, Sotiriadis K, Skaropoulou A. Thaumasite form of sulfate attack (TSA) in limestone cement pastes. Ref Reports IX Conf Exhib Eur Ceram Soc 2007;27:1711–4. doi:https://doi.org/10.1016/j.jeurceramsoc.2006.05.048.